Reinvestigation of the Layered Double Hydroxide Containing Tetravalent Cations: Unambiguous Response Provided by XAS and Mössbauer Spectroscopies

Mourad Intissar,[†] Jean-Claude Jumas,[‡] Jean-Pierre Besse,[†] and Fabrice Leroux*,[†]

Laboratoire des Matériaux Inorganiques, UMR 6002-CNRS, Université Blaise Pascal, 24 av. des Landais, 63177 Aubière cédex, France, and Laboratoire des Agrégats Moléculaire et Matériaux Inorganiques, UMR 5072-CNRS, Université Montpellier II, place Eugène Bataillon, 34095 Montpellier cédex 5, France

Received May 20, 2003. Revised Manuscript Received September 5, 2003

The incorporation of tetravalent cations (Zr^{4+} and Sn^{4+}) inside sheets of layered double hydroxide (LDH) was reported by Velu et al. As no local structural information was provided so far, the question here is whether the LDH structure may accommodate such a presence. From three different systems presenting the cation compositions MgAlSn, MgAlZr, and CoAlSn, we provide (by means of X-ray absorption and Mössbauer spectroscopies) clear evidence that the tetravalent cations are segregated from the LDH structure and form amorphous M^{IV} oxide-like particles. Variation of the cell parameters, ***a*** and ***c***, is then explained by a substitution of Al cations by the divalent cations, M^{II}. It is also shown that despite the fact that the process of reconstruction occurs for MgAlM (M = Zr and Sn), the tetravalent cations do not participate in this structural recovery.

1. Introduction

There is growing interest in layered double hydroxide-type materials (LDH) due to their potential application in numerous domains[1] such as in green chemistry, as precursors for catalysts, etc.

The LDH structure is referred to the natural hydrotalcite, and described with the ideal formula, $[M^{II}_x M_{1-x}^{III}(OH)_2]_{intra}[A^{m-}_{x/m}. nH_2O]_{inter}$, where M^{II} and M^{III} are metal cations, *A* represents the anions, and intra and inter denote the intralayer domain and the interlayer space, respectively. The structure consists of brucite-like layers constituted of edge-sharing $M(OH)_6$ octahedra.[2] Partial M^{II} to M^{III} substitution induces a positive charge for the layers, balanced with the presence of the interlayered anions.

From the incorporation of Pd^{2+} or Pt^{2+} within LDH sheets, the materials were considered as useful precursors of noble-metal-containing heterogeneous catalysts;[3] other studies report the presence of Ru^{3+}, Rh^{3+}, and Ir^{3+} in LDH samples.[4]

In 1997, Velu et al. reported the possibility of incorporating tetravalent cations into LDH-type layers, and this was demonstrated for M^{IV} = Zr and Sn with two LDH frameworks, Mg_3Al and Co_3Al, over a large composition range.[5,6] Indeed, the authors claimed that up to 30% of Al^{3+} could be isomorphously substituted by Sn^{4+} to form a new MgAlSn ternary LDH.[6]

XRD, FTIR, and TG analysis were combined to characterize the samples and to picture the trend. The crystallinity of the material was found to decrease with increasing M^{IV} content, this was explained by structural distortions introduced by the incorporation of the larger cation.

The acido-basic properties and reducibility of the mixed oxides formed upon calcination were recently studied.[7] Even though the physicochemical properties and some catalytic performances have been reported for these LDH "derivatives", no detailed structural local picture has been supplied for the incorporation of M^{IV} cations into hydrotalcite type layers so far. The question is whether the M^{IV} cations are accommodated within LDH sheets taking into account their size and charge, and considering SnO_2-type xerogels are known to be synthesized in basic medium.[8] In our case, using a similar preparation but in the absence of both Al and divalent cation, an amorpous sample is obtained from Zr and Sn tetravalent cation source.

* To whom correspondence should be addressed. E-mail: fleroux@chimtp.univ-bpclermont.fr.

[†] Université Blaise Pascal.

[‡] Université Montpellier II.

(1) De Roy, A.; Forano, C.; El Malki, K.; Besse, J.-P. *Synthesis of Microporous Materials*; Occelli, M. L., Robson, H. E., Eds.; Van Nostrand Reinhold: New York, 1992; vol. 2, p 108.

(2) Allman, R. *Chimia* **1970**, *24*, 99. Thiel, J. P.; Chiang, C. K.; Poeppelmeier, K. R. *Chem. Mater.* **1993**, *5*, 297. Besserguenev, A. V.; Fogg A. M.; Price, S. J.; Francis, R. J.; O'Hare, D.; Isupov, V. P.; Tolochko, B. P. *Chem. Mater.* **1997**, *9*, 241.

(3) Basile, F.; Fornasari, G.; Gazzano, M.; Vaccari, A. *Appl. Clay Sci.* **2000**, *16*, 185.

(4) Basile, F.; Fornasari, G.; Gazzano, M.; Vaccari, A. *J. Mater. Chem.* **2002**, *12*, 3296.

(5) (a) Velu, S.; Ramaswamy, V.; Ramani, A.; Chanda, B. M.; Sivasanker, S. *Chem. Commun.* **1997**, 2107. (b) Velu, S.; Sabde, D. P.; Shah, N.; Sivasanker, S. *Chem. Mater.* **1998**, *10*, 3451. (c) Velu, S.; Suzuki, K.; Osaki, T.; Ohashi, F.; Tomura, S. *Mater. Res. Bull.* **1999**, *34*, 1707.

(6) Velu, S.; Suzuki, K.; Okazaki, M.; Osaki, T.; Tomura, S.; Ohashi, T. *Chem. Mater.* **1999**, *11*, 2163.

(7) (a) Velu, S.; Suzuki, K.; Kapoor, M. P.; Tomura, S.; Ohashi, F.; Osaki, T. *Chem. Mater.* **2000**, *12*, 719. (b) Tichit, D.; Das, N.; Coq, B.; Durand, R. *Chem. Mater.* **2002**, *14*, 1530.

(8) Briois, V.; Santilli, C. V.; Pulcinelli, S. H.; Brito, G. E. S. *J. Non-Cryst. Solids* **1995**, *191*, 17.

10.1021/cm0304039 CCC: $25.00
Published on Web 10/22/2003

Prepared as previously described by Velu et al.,[5−7] the different samples of cation compositions Mg_3(Al, Zr), Mg_3(Al, Sn), and Co_3(Al, Sn) were prepared and characterized. Our results concerning X-ray diffraction patterns, FTIR spectra, and thermal behavior are in agreement with what was previously published in the literature. In a next step, X-ray absorption and ^{119}Sn Mössbauer spectroscopies were used to scrutinize the local arrangement. Both techniques are highly selective; XAS was largely employed for the determination of the local order of elements in relatively small amounts such as for chromium-promoted tin^{IV} oxide catalysts,[9] manganese-oxo[10] or Zr species into MCM-41[11] channels, for the crystallite growth of nanocrystalline copper-doped tin oxide,[12] or incorporated in SNAPO-5 tin-substituted aluminophosphate zeolite,[13] for zirconia[14] or titania−silica xerogels.[15]

In the present study, the fine structures at the K-edge of Co, Zr, and Sn were analyzed. The moduli of the Fourier transform are compared to the theoretical model.

2. Experimental Section

2.1. Preparation of the Samples. $SnCl_4 \cdot 5H_2O$ (Acros), $ZrO(NO_3)_2 \cdot xH_2O$ (Aldrich, $x = 6.05$ determined by TG analysis), $Mg(NO_3)_2 \cdot 6H_2O$ (Acros, 99%), $Co(NO_3)_2 \cdot 6H_2O$ (Aldrich, 99%), $Al(NO_3)_3 \cdot 9H_2O$ (Acros, 99%), NaOH (Acros, 97%), $Na_2CO_3 \cdot 10H_2O$ (Acros, 99%) were used as received.

All the hydrotalcite-like materials were prepared by the coprecipitation method according to Miyata.[16] Experimentally, 250 mL of a solution of the salts M^{II}(3×10^{-2} M), Al ($4(0.25 - y) \times 10^{-2}$ M), and M^{IV} ($4y \times 10^{-2}$ M) of desired cation ratio was added dropwise to a solution of mixed NaOH (2 M) and Na_2CO_3 (0.3 M), as described by Velu et al.[5−7]

The pH was kept constant during the addition: pH 10 ± 0.1 for the system $Mg_{0.75}Al_{0.25-y}M_y$ (M = Zr and Sn) and 9 ± 0.1 for $Co_{0.75}Al_{0.25-y}Sn_y$. The slurry was aged overnight, centrifuged, washed several times with distilled water, and finally dried at room temperature.

Similar procedures were used in the absence of Al and divalent cation sources. For Zr and Sn, an amorphous precipitate was obtained.

2.2. Techniques of Characterization. Powder X-ray diffraction profiles (PXRD) were obtained with a Siemens D500 X-ray diffractometer with a diffracted beam monochromator Cu Kα source.

2.3. X-ray Absorption Spectroscopy. *2.3.1. Co, Zr, and Sn K-Edge.* XAS studies were performed at LURE (Orsay, France) using X-ray synchrotron radiation emitted by the DCI storage ring (1.85 GeV positrons, average intensity of 250 mA) at the D44 beam line. Data were collected at 77 K in transmission mode at the Co, Zr, and Sn K-edge (7708.9, 17 997.6, and 29 200.0 eV, respectively). For Co K-edge, a double-crystal Si (111) monochromator scanned the energy in 2-eV steps from 100 eV below to 900 eV above each K-edge, and three spectra were recorded for each sample. An accumulation time of 2 s was used per point. For Zr and Sn, a double-crystal Ge (400) was used, and the recording conditions were 4 eV for the step and 2 s per point.

Extraction and analysis of EXAFS data was performed following standard procedures as reported elsewhere.[17] The $\chi(k)$ signal was fitted by using the classical plane-wave single scattering approximation: $\chi(k) = S_0^2 \Sigma A_i(k) \times \sin[2kr_i + \phi_i(k)]$, with $A_i(k)$ amplitude equal to $(N_i/k(r_i)^2)F(k) \times \exp(-2k^2\sigma_i^2) \times \exp(-2r_i/\Gamma)$, where r_i is the interatomic distance, ϕ_i is the total phase shift of the ith shell, N_i is the effective coordination number, σ_i is the Debye−Waller factor, $F_i(k)$ is the backscattering amplitude, and Γ is the free-mean path. To estimate the relative part of the cations contributing to the metal−metal correlation, the number of backscattering atoms was free to move during the refinement. This guarantees all possible cation ratios for the second shell. ZrO_2, SnO_2, Co_2SnO_4, Mg_2SnO_4, $CoAl_2O_4$, and $Co(OH)_2$ were taken as reference compounds. All results were similar using FEFF 8 for MAC.

2.3.2. Mg K-Edge (1305.0 eV). Data were collected at room temperature in total yield electron mode at the SA 32 beamline at LURE, using the SuperAco positron storage ring. A double-crystal Ge (111) monochromator scanned the energy in 1-eV steps from 1250 to 1560 eV, and three spectra were recorded for each sample. The accumulation time was 1 s per point. The standard procedures for the extraction of the signal are described above, however, the small domain in Δk (2.2 to 7.5 Å^{-1}) due to the presence of the Al K-edge (1559 eV) is not satisfactory for the procedures of refinement.

2.4. Mössbauer Spectroscopy. ^{119}Sn Mössbauer spectra were recorded by transmission in the constant acceleration mode using an EG&G spectrometer, equipped with a cryostat to work at low temperature (down to 4 K). The absorbers, containing 1−2 mg of ^{119}Sn per cm^2, were prepared by mixing powder samples and Apiezon grease inside the glovebox, and sealed with Parafilm to avoid contact with air. The source was ^{119m}Sn in a $BaSnO_3$ matrix of nominal activity 10 mCi. The velocity scale was calibrated using the magnetic sextet of a high-purity iron foil absorber as a standard, using ^{57}Co (Rh) as the source. The spectra were fitted to Lorentzien profiles by least-squares method using the ISO program,[18] and the fit was quality controlled by the classical χ^2 test. Isomer shift values are given relative to the center of the $BaSnO_3$ spectrum recorded at room temperature.

3. Results and Discussion

3.1. Hypothesis of Substitution. *3.1.1. Chemical Formulas.* In the following, two hypotheses are considered. The first considers the substitution $M^{III} - M^{IV}$ effective, then the LDH composition is a function of the M^{IV} cations content, y in $M^{II}_{0.75}Al_{0.25-y}M^{IV}_y(OH)_2(CO_3)_{(y+0.25)/2} \cdot nH_2O$. The second is to surmise that the substitution $M^{III} - M^{IV}$ is not effective, and that it involves merely a change in the M^{II}/M^{III} cation ratio. In the latter case, the composition is a function of x, M^{III} content, and the formula becomes $M^{II}_{1-x}Al_x(OH)_2(CO_3)_{x/2} \cdot nH_2O$.

The x and y values are calculated from the chemical analysis data as follows:

$$x = 1/(1 + \beta_{exp}) \text{ with } \beta_{exp} = M^{II}/Al \quad (1)$$

$$y = 0.25^*\alpha_{exp}/(1 + \alpha_{exp}) \text{ with } \alpha_{exp} = M^{IV}/Al \quad (2)$$

The chemical analyses of the different samples are summarized in Table 1.

(9) Harrison, P. G.; Lloyd, N. C.; Daniell, W.; Bailey, C.; Azelee, W. *Chem. Mater.* **1999**, *11*, 896.
(10) Burch, R.; Cruise, N. A.; Gleeson, D.; Tsang, S. C. *J. Mater. Chem.* **1998**, *8*, 227.
(11) Morey, M. S.; Stucky, G. D.; Schwarz, S.; Fröba, M. *J. Phys. Chem. B* **1999**, *103*, 2037.
(12) Santilli, C. V.; Pulcinelli, S. H.; Brito, G. E. S.; Briois, V. *J. Phys. Chem. B* **1999**, *103*, 2660.
(13) Flavell, W. R.; Nicholson, D. G.; Nilsen, M. H.; Stahl, K. *J. Mater. Chem.* **2001**, *11*, 620.
(14) Mountjoy, G.; Pickup, D. M.; Anderson, R.; Wallidge, G. W.; Holland, M. A.; Newport, R. J.; Smith, M. E. *Phys. Chem. Chem. Phys.* **2000**, *2*, 2455.
(15) Pickup, D. M.; Mountjoy, G.; Wallidge, G. W.; Anderson, R.; Cole, J. M.; Newport, R. J.; Smith, M. E. *J. Mater. Chem.* **1999**, *9*, 1299.
(16) Miyata, S. *Clays Clay Miner.* **1980**, *28*, 50.
(17) Leroux, F.; Piffard, Y.; Ouvrard, G.; Mansot, J-.L.; Guyomard, D. *Chem. Mater.* **1999**, *11*, 2948.
(18) Kündig, W. *Nucl. Instrum. Methods* **1979**, *75*, 336.

Table 1. Cation Composition and Cell Parameter *a* for the Samples

system $M^{II}/Al/M^{IV}$	α_{exp}	y	β_{exp}	x	$\boldsymbol{a}$ (Å)^{ref}
		system MgAlZr			
2.9/1.1/0	0	0	2.64	0.275	3.050 [7]
2.84/0.88/0.27	0.307	0.059	3.22	0.236	3.043[7]
2.6/1.14/0.26	0.228	0.046	2.28	0.305	3.023[7]
3/0.96/0	0	0	3.12	0.24	3.0588 [5b]
3/0.85/0.07	0.08	0.018	3.53	0.22	3.0632[5b]
3/0.78/0.14	0.18	0.038	3.85	0.206	3.0688 [5b]
3/0.68/0.21	0.31	0.059	4.41	0.185	3.0688[5b]
3/0.67/0.33	0.49	0.082	4.47	0.182	3.0732[5b]
3/0.57/0.37	0.65	0.098	5.26	0.159	3.0768[5b]
3/0.52/0.50	0.96	0.122	5.77	0.148	3.078[5b]
0.75/0.26/0	0	0	2.88	0.257	3.045[a]
0.75/0.24/0.03	0.125	0.028	3.12	0.242	3.053[a]
0.75/0.25/0.06	0.24	0.048	3.00	0.250	3.058[a]
0.75/0.16/0.09	0.56	0.090	4.68	0.176	3.0692[a]
0.75/0.13/0.12	0.92	0.120	5.77	0.148	3.0734[a]
0.75/0.06/0.19	2.68	0.182	5.68	0.149	3.0776[a]
		system MgAlSn			
3/0.9/0	0	0	3.33	0.23	3.053[6, 5c]
3/0.8/0.09	0.1125	0.025	3.75	0.21	3.056[6, 5c]
3/0.71/0.19	0.267	0.052	4.22	0.191	3.064[6, 5c]
3/0.70/0.29	0.414	0.073	4.28	0.189	3.067[6, 5c]
3/0.54/0.37[b]	0.685	0.101	5.55	0.152	3.082[6, 5c]
3/0.44/0.45[b]	1.023	0.126	6.82	0.128	3.091[6, 5c]
0.75/0.26/0	0	0	2.88	0.257	3.045[a]
0.75/0.21/0.04	0.19	0.040	3.57	0.218	3.058[a]
0.75/0.19/0.081	0.433	0.075	4.01	0.199	3.068[a]
		system CoAlSn			
3/0.86/0	0	0	3.48	0.223	3.074[7]
3/0.93/0.36	0.387	0.070	3.22	0.237	3.103[7]
0.75/0.24/0	0	0	3.125	0.242	3.078[a]
0.75/0.22/0.04	0.182	0.038	3.409	0.227	3.0851[a]
0.75/0.17/0.07	0.412	0.073	4.412	0.185	3.0942[a]
0.75/0.14/0.11	0.786	0.110	5.357	0.157	3.0954[a]

[a] This work. [b] Phases mixture.

3.1.2. X-ray Diffraction. X-ray diffraction patterns are displayed in Figure 1; they are typical of the layered double hydroxide structure. For the starting LDH composition ($y = 0$), the reflections were indexed in a hexagonal lattice with a $R\bar{3}m$ rhombohedral symmetry, commonly used for the description of the LDH structure. Miller indexation is given in Figure 1. From these structural considerations, the cell parameters are given by

$$\boldsymbol{a} = 2 \times d_{110} \text{ and } \boldsymbol{c} = 3 \times d_{003} \text{ (or } 6 \times d_{006})$$

For all the studied systems, the apparent incorporation of tetravalent cations induces a decrease in crystallinity, as the diffraction lines become wider, (110) and (113) are lumped together. Concerning the system MgAlZr, for ($^{x}/_{y}$) of ($^{0.15}/_{0.18}$), the harmonics are barely observed, and the samples turn amorphous for greater values of y. It was hypothesized that the loss of crystallinity may be due to the co-formation of amorphous Zr and Mg salts, however, a precipitate is still formed in the absence of a Mg source.

In the case of the system MgAlSn, the magnesium hydroxostannate phase $MgSn(OH)_6$ is observed for y greater than 0.075, as mentioned by Velu et al.[6]

For CoAlSn and ($^{x}/_{y}$) over ($^{0.16}/_{0.11}$), the phases present silent XRD diagram.

FTIR spectra and thermal behavior of the different phases are in agreement with the data published in the literature, however, they are not relevant to ascertain the location of the tetravalent cations.

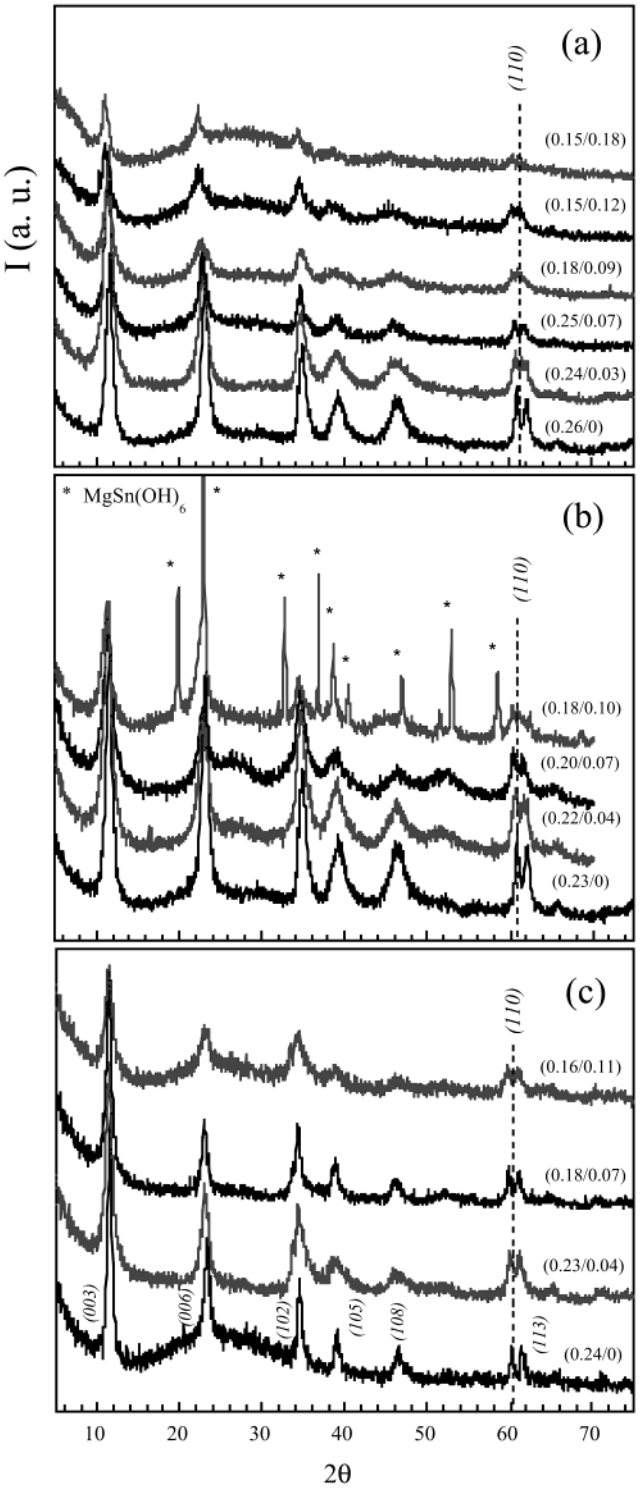

Figure 1. X-ray patterns of the synthesized LDH materials of cation composition (a) MgAlZr, (b) MgAlSn, and (c) CoAlSn. Given the two hypotheses for the substitution, $M^{II} - M^{III}$ ($M^{II}_{1-x}Al_x$) or $M^{III} - M^{IV}$ ($Al_{1-y}M^{IV}_y$), the values of (x, y) are reported.

3.1.3. Variation of Cell Parameter. At first glance, and as surmised by previous authors, the substitution $M^{III} - M^{IV}$ seems to occur, and the tetravalent cations seem to be readily incorporated into LDH sheets as a shift of the diffraction line (110) is observed for each studied system. This implies that the cell parameter $\boldsymbol{a}$ is modified. However, the question is to determine the origin of these modifications. It is occurring effectively from the incorporation of the M^{IV} cations or merely due

to a substitution of M^{III} by M^{II} cations, with the relative content of M^{III} cations being lowered when y is increased.

In a first approximation, the expected cell parameter variation may be calculated assuming Vegard's law and an ideal atomic arrangement for the cations.[19] From an ideal *in-plane* octahedra assembly, the size of the octahedra sharing edges is related to the metal−oxygen distance by the relation $\boldsymbol{a} = \sqrt{2} \times d(M-O)$ and the latter to the ionic radii by the relation

$$d_x(M-O) = (1 - x) \times r(M^{II}) + x \times r(M^{III}) \quad (3)$$

in the hypothesis of a substitution $M^{II} - M^{III}$, and

$$d_y(M-O) = 0.75 \times r(M^{II}) + (0.25 - y) \times r(M^{III}) + y \times r(M^{IV}) \quad (4)$$

for $M^{III} - M^{IV}$ substitution. Finally, the variation of the crystalline parameter $\boldsymbol{a}$ content is given respectively by

$$\delta\boldsymbol{a}/\delta x = -\sqrt{2} \times [r(M^{II}) - r(M^{III})] \quad (5)$$

and

$$\delta\boldsymbol{a}/\delta y = \sqrt{2} \times [r(M^{IV}) - r(M^{III})] \quad (6)$$

The ionic radii of the different elements are taken from the usual database.[20]

From the data listed in Table 1, both hypotheses are presented in Figures 2 and 3.

The expected slopes corresponding to $\delta\boldsymbol{a}/\delta y$ and $\delta\boldsymbol{a}/\delta x$ from relations 5 and 6 are materialized as a dashed line in Figures 2 and 3, respectively. The second hypothesis (substitution $M^{II} - M^{III}$) appears to be slightly more consistent with the experimental data gathered from the different sources, however, it is more pronounced for the system MgAlZr.

In the case of the substitution $M^{II} - M^{III}$ (Figure 3), it would suggest that the LDH structure MgAl and CoAl may be stabilized with low Al content, from 2.8 to 5.7, and 3.1 to 5.3 for β in $M^{II}{}_{\beta}Al$, M^{II} = Mg or Co, respectively. A larger domain of substitution, $\beta_{exp} = M^{II}/Al$ up to 7.7, was found for the system GaAl.[21] Nevertheless, an amorphous component is observed on the XRD patterns for the materials presenting large values for y ($y > 0.09$ (or $x < 0.18$)), which may be attributed to M^{IV} oxide and other amorphous phases resulting from the high M^{II} content. In the latter case, this may explain the slight deviation of the cell parameter at this regime (Figures 2 and 3). Note that the spectroscopic characterizations will analyze the whole, although, because no sudden evolution is observed (vide infra), one can surmise that the second amorphous portion (other than M^{IV} oxide) is small and has a weak effect on the results.

3.2. Local Study by Spectroscopy. *3.2.1. XAS Study.* To shed some light on these discrepancies, the samples were studied by XAS technique. The cation ordering requires structural conditions for establishing the local order. From an ideal model with a ratio M^{II} to M^{III} of 3, the M^{II} cations must be surrounded by $4M^{II}$ and $2M^{III}$, whereas $6M^{II}$ are present in the close vicinity of the polyhedra $M^{III}(OH)_6$.[19] This local order was observed for several LDH-type materials, such as pyroaurite Mg_2Fe,[22] Cu_2Cr,[23] and Co_3Al.[24] In all of the

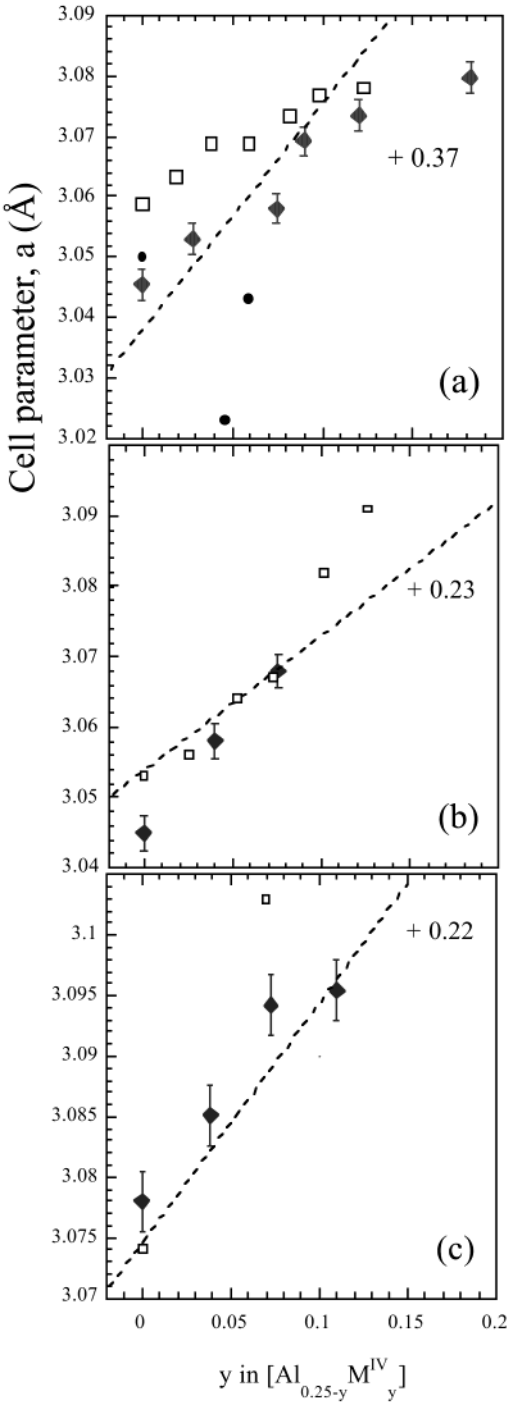

Figure 2. Comparison of the cell parameter, $\boldsymbol{a}$, between experimental and expected data in the hypothesis of the substitution $M^{III} - M^{IV}$for (a) MgAlZr, (b) MgAlSn, and (c) CoAlSn. The experimental data are as follows: open square from Velu et al., black circle from Tichit et al., and gray diamonds from this work. The expected data are visualized by the dashed lines (see text).

(19) Hofmeister, W.; Von Platen, H. *Cryst. Rev.* **1992**, *3*, 3.
(20) Handbook of Physics, ed. 2001.
(21) Lopez-Salinas, E.; Garcia-Sanchez, M.; Montoya, J. A.; Acosta, D. R.; Abasolo, J. A. Schifter, I. *Langmuir* **1997**, *13*, 4748.
(22) Vucelic, M.; Jones, W.; Moggridge, G. D. *Clays Clay Miner.* **1997**, *45*, 803.
(23) Roussel, H.; Briois, V.; Elkaïm, E.; de Roy, A.; Besse, J.-P.; Jolivet, J.-P. *Chem. Mater.* **2001**, *13*, 329.
(24) Intissar, M.; Segni, R.; Payen, C.; Besse, J.-P.; Leroux, F. *J. Solid State Chem.* **2002**, *167*, 508.

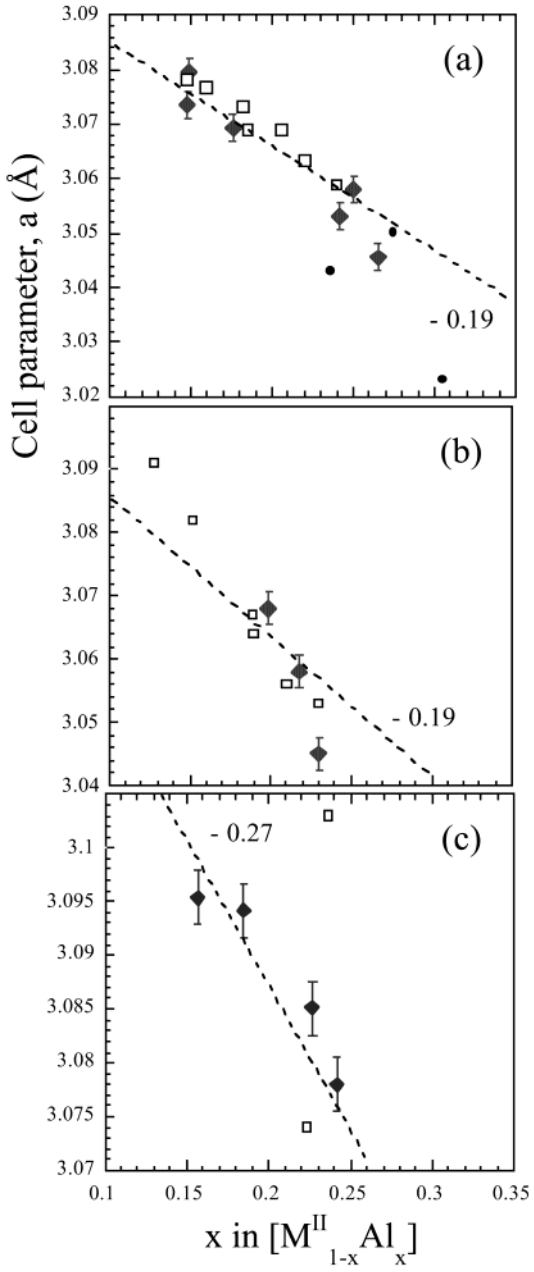

Figure 3. Comparison of the cell parameter, ***a***, between experimental and expected data in the hypothesis of the substitution $M^{II} - M^{III}$ for (a) MgAlZr, (b) MgAlSn, and (c) CoAlSn. The experimental data are as follows: open square from Velu et al., black circle from Tichit et al., and gray diamonds from this work. The expected data are visualized by the dashed lines (see text).

studies, no correlation between trivalent cations was observed.

For Sn^{IV} cations located inside LDH sheets, we surmise that their local environment must fulfill at least two conditions: (i) no short Sn−Sn correlation, which would imply the presence of a segregation between LDH and Sn-based entities, and (ii) Sn−M^{II} correlation at a distance of ***a***, as expected for LDH.

3.2.1.1. System CoAlSn. The FT moduli are displayed in Figure 4 at Co and Sn K-edge. The features of the FT moduli at the Co K-edge are characteristic of a LDH phase, namely the peak P1 represents the contribution Co−O, the contributions at longer distances arise from multiple scattering effects and are attributed to metallic

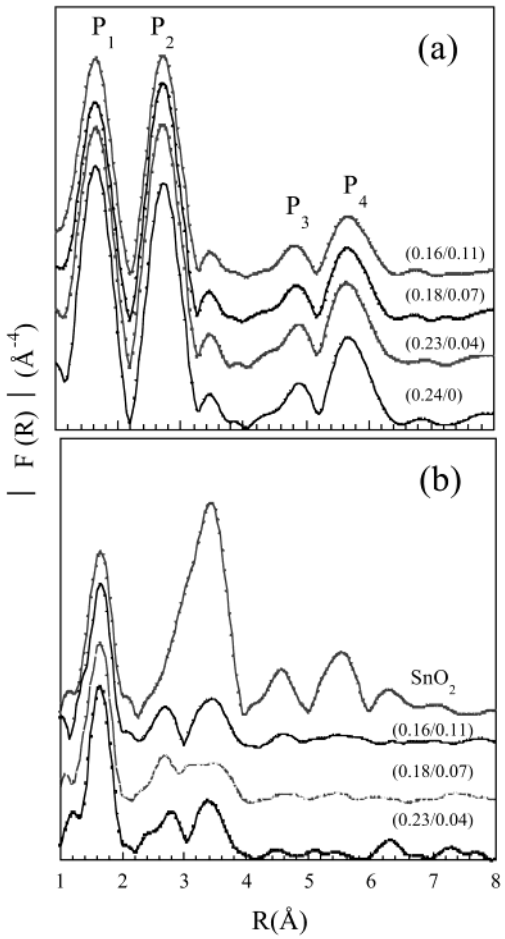

Figure 4. Moduli of the Fourier transform for CoAlSn LDH system at (a) Co K-edge and (b) Sn K-edge. The samples are referred according to Table 1. The distances are not corrected from phase shifts.

neighbors, P2 at a distance of ***a***, P3 at a distance of $\boldsymbol{a}\sqrt{3}$, and P4 at a distance of $2\boldsymbol{a}$. The latter is largely enhanced by the so-called focusing effect due to three atoms lying linearly from each other.[25] The observation of P4 implies the presence of flat inorganic sheets, inversely their absence would have been explained by the presence of corrugated layers. Rather small offsets in the linearity are enough to detune and lose the P4 amplification.

At Sn K-edge, the structural local picture is different and the two contributions P3 and P4 are not observed. Consequently, it suggests that there is no Sn-surrounding atom lying linearly from each other, regardless of the values of *y*. For P2, a double structure is observed with two distinct Sn−Sn refined distances (Table 2). The contributions look like those encountered for hydrogels or xerogels of SnO_2 rutile-type samples.[8] This, added to the fact that no correlation of Sn−Co is expected at a distance of ***a***, suggests strongly that Sn atoms are not located in LDH sheets, thus dismissing the hypothesis of Al substitution by Sn cations.

The distance Sn−O is fitted with six oxygen atoms and two different shells Sn−Sn (Table 2).

3.2.1.2. Systems MgAlM (M = Zr and Sn). For MgAlSn, the FT moduli at Sn K-edge (Figure 5b) are similar to those presented for CoAlSn (Figure 4b). The

(25) Alberding, N.; Crozier, E. D. *Phys. Rev. B* **1983**, *27*, 3374.

Table 2. XAS Fit Results and Crystallographic Data for Reference Samples[a]

compound	correlation	N	R (Å)	σ^2 (10^{-3} Å^2)	ρ^b(%)
ZrO_2[c]	Zr−O	5	2.11	3.6	
	Zr−O	2	2.26	3.6	
	Zr−Zr	7	3.45	7	6
	system MgAlZr ($^x/_y$)[d]				
(0.24/0.03)	Zr−O	5.1	2.15	3.5	
	Zr−O	3.0	2.28	3.5	
	Zr−Zr	2.4	3.49	10	8
(0.18/0.09)	Zr−O	5.2	2.15	3.5	
	Zr−O	3	2.20	3.5	
	Zr−Zr	3.8	3.50	12	8
(0.15/0.18)	Zr−O	4.1	2.14	3.5	
	Zr−O	3.0	2.28	3.5	
	Zr−Zr	2.8	3.49	13	5
SnO_2[e]	Sn−O	6	2.05	6.4	
	Sn−Sn	2	3.18	7.3	
	Sn−Sn	8	3.71	5.6	9
	system MgAlSn ($^x/_y$)[d]				
(0.22/0.04)	Sn−O	6.0	2.07	5.5	3.5
	Sn−Sn	2.0	3.18	8.8	
	Sn−Sn	2.5	3.74	15	
(0.20/0.07)	Sn−O	5.8	2.07	5.5	
	Sn−Sn	2.0	3.18	8.6	
	Sn−Sn	3.0	3.74	14.3	5.5
$CoAl_2O_4$[f]	Co−O	4.1	1.92	4.3	
	Co−Al	9.3	2.87	6.4	
	Co−Co	0.8	2.89	7.2	
	Co−Co	6.1	3.36	9.0	3
	system CoAlSn ($^x/_y$)[d]				
(0.24/0.0)	Co−O	6.0	2.06	6.4	
	Co−Co	4.3	3.10	7.5	
	Co−Al	3.0	3.03	8.6	4
(0.23/0.04)	Co−O	6.0	2.06	6.4	
	Co−Co	4.3	3.11	7.5	
	Co−Al	3.0	3.03	8.6	2
(0.18/0.07)	Co−O	5.9	2.06	7.8	
	Co−Co	4.5	3.11	8.1	
	Co−Al	2.4	3.04	9.14	1.5
(0.16/0.11)	Co−O	6.0	2.06	7.9	
	Co−Co	4.7	3.10	8.9	
	Co−Al	2.7	3.02	9.1	1
(0.23/0.04)	Sn−O	6.2	2.07	6.0	
	Sn−Sn	1.0	3.20	9.1	
	Sn−Sn	2.8	3.73	7.8	9
(0.18/0.07)	Sn−O	6.5	2.07	6.3	
	Sn−Sn	1.0	3.20	8.0	
	Sn−Sn	2.35	3.73	7.5	9
(0.16/0.11)	Sn−O	6.3	2.07	5.4	
	Sn−Sn	1.0	3.19	7.8	
	Sn−Sn	3.3	3.72	8.4	9

[a] Co_2SnO_4 and Mg_2SnO_4 crystallize in space group $Fd\bar{3}m$ with a cubic symmetry. Because there is no correlation observed between Sn and divalent cation, their corresponding refinements are not presented. [b] The residual ρ factor is defined as $\rho = [\Sigma(k^3\chi_{exp}(k) - k^3\chi_{theo}(k))^2/\Sigma(k^3\chi_{exp}(k))^2]^{1/2}$. The commonly accepted fitting accuracy is about 0.02 Å for the distance and 15 to 20% for the number of neighbors. [c] From structural data. ZrO_2 crystallizes in space group $P121/c$ (14) with monoclinic symmetry, lattice parameters of $\boldsymbol{a} = 5.148$ Å, $\boldsymbol{b} = 5.208$ Å, $\boldsymbol{c} = 5.315$ Å, and $\beta = 99.2°$. Distances in ZrO_2: first coordination sphere, Zr−O = 2.044, 2.064, 2.135, 2.137, 2.169, 2.254, and 2.269 Å; nearest Zr−Zr = 3.338, 3.447 (2), 3.462 (2), 3.478, and 3.573 Å. [d] Taking into account both hypotheses: $x = 1/(1 + \beta_{exp})$ with $\beta_{exp} = M^{II}/Al$, and $y = 0.25\alpha_{exp}/(1 + \alpha_{exp})$ with $\alpha_{exp} = M^{IV}/Al$ (see text). [e] From structural data. SnO_2 crystallizes in space group $P42/mnm$ (136) with tetragonal symmetry, lattice parameters of $\boldsymbol{a} = 4.736$ Å and $\boldsymbol{c} = 3.185$ Å. Distance in SnO_2: Sn−O = 2.045 (2) and 2.058 (4) Å, and Sn−Sn = 3.185 (2) and 3.708 (8) Å. [f] From structural data. $CoAl_2O_4$ cristallizes in $Fd\bar{3}m$ space group with a cubic symmetry, lattice parameter of $\boldsymbol{a} = 8.107$ Å. Co(1) and Al(1) in 8a symmetry (−43m), Co(2) and Al(2) in 16d (−3m), O in 32e (3m), and with an occupancy rate of [0.849] and [0.0755] for Co(1) and Co(2), respectively, and [0.151] and [0.9245] for Al(1) and Al(2), respectively, giving rise to $2\{0.849Co(1) + 0.151Al(1)\} + 4\{0.0755Co(2) + 0.9245Al(2)\} = Co_2Al_4O_8$.[26] Taking into account the rate occupancy and the difference of site for Co(1) and Co(2), the average oxygen coordination around Co is 4.25 Co at 1.93 Å, and the environment Co−Me is described as follows: 5.7 Al^{3+} at 2.866 Å, 0.5 Co^{2+} at 2.866 Å, and 6.4 Co^{2+} at 3.361 Å.

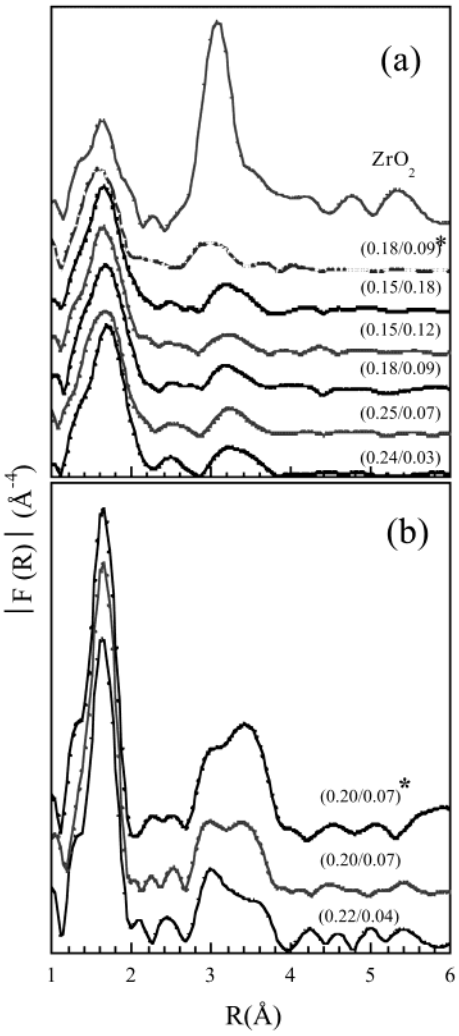

Figure 5. Moduli of the Fourier transform for (a) MgAlZr and (b) MgAlSn LDH systems at Zr K-edge and Sn K-edge, respectively. The samples are referred according to Table 1. The distances are not corrected from phase shifts. The asterisks designate the phases obtained after treatment at 400 °C and reconstruction.

results of the refinement are reported in Table 2. As before, one can conclude that the Sn^{IV} cations are not located inside MgAl sheets and that the substitution of Al by Sn cations is not effective.

For MgAlZr, the FT moduli at Zr K-edge are displayed in Figure 5a. As before, the features of the moduli are not characteristic of a LDH framework. The refined distances Zr−O and Zr−Zr are close to those present in ZrO_2 (Table 2).

For Zr or Sn-containing samples, the FT moduli at Mg K-edge present features similar to one another, and also similar to those of the LDH material Mg_3Al (Figure 6). It shows the absence of backscatterers, such as Zr and Sn, in the close environment of Mg atoms. In such a case as for Mg_2SnO_4, which crystallizes in the space group $Fd\bar{3}m$ with the cell parameter $a = 8.639$ Å and which presents a closest distance Mg−Sn of 3.054 Å,[27] a large contribution is observed on the FT curve (Figure 6).

(26) Leroux, F.; El Moujahid, M.; Roussel, H.; Flank, A.-M.; Briois, V.; Besse, J.-P. *Clays Clay Miner.* **2002**, *50*, 254.
(27) Poix, P. *Annales Chim.* **1964**, 261.

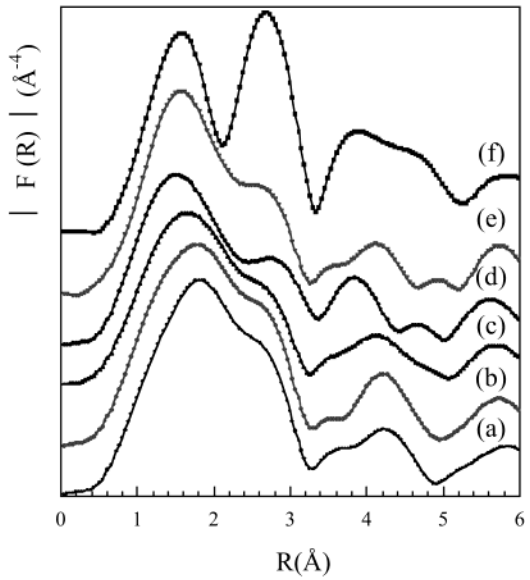

Figure 6. Moduli of the Fourier transform at Mg K-edge of the samples MgAl (a) (0.23/0), MgAlSn (b) (0.22/0.04) and (c) (0.20/0.07), and MgAlZr (d) (0.24/0.03) and (e) (0.18/0.09), and of (f) Mg_2SnO_4. The distances are not corrected from phase shifts.

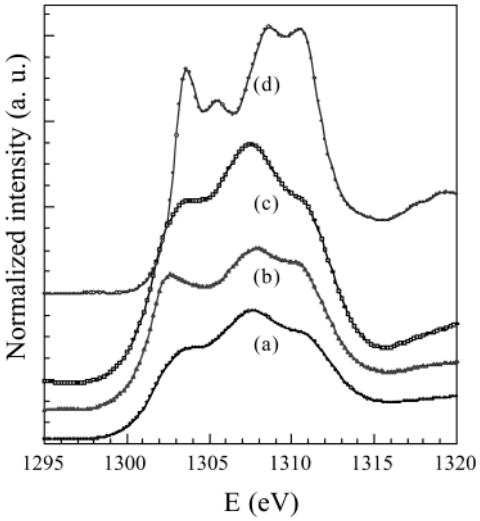

Figure 7. XANES curves at Mg K-edge for MgAlZr (0.18/0.09) at (a) 25 °C, (b) after treatment at 400 °C, (c) after reconstruction, and (d) for MgO.

MgAl-based LDHs are found to be recovered after thermal treatment.[28] During this treatment, the LDH phase turns amorphous, and the local environment surrounding the Mg atoms resemble that of MgO (Figure 7), in agreement with previous observations.[29] When placed in carbonate solution and dried, the material presents a FT modulus at Mg K-edge similar to that of the pristine form. This is not the case at either Zr or Sn K-edge, as the contact between cations is irreversibly shortened (Figure 5 a and b, curves marked by a asterisk). This shows that the tetravalent cations do not participate in the process of reconstruction, although it occurs for both systems with cell parameters similar to those of the pristine phase.

(28) Hibino, T.; Tsunashima, A. *Chem. Mater.* **1998**, *10*, 4055.
(29) Bokhoven, J. A.; Roelofs, J. C. A. A.; de Jong, K.; Koningsberger, D. C. *Chem. Eur. J.* **2001**, *7*, 1258.

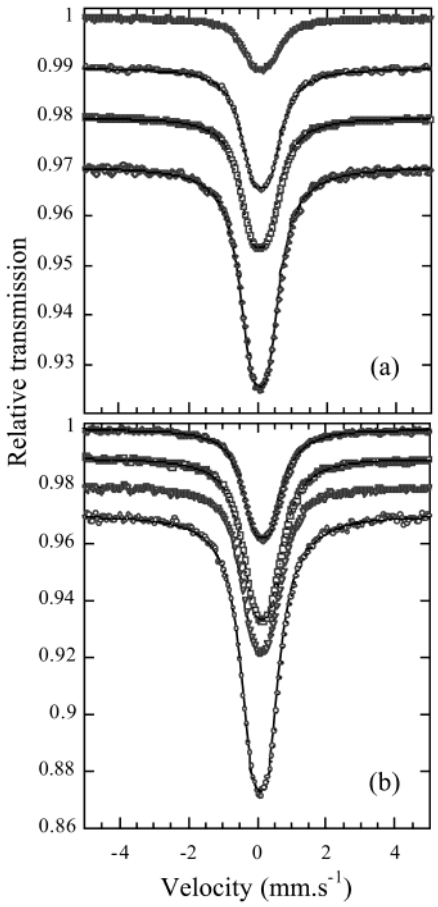

Figure 8. Mössbauer spectra of the Sn-containing samples recorded at (a) 293 K and (b) 80 K, from top CoAlSn (0.23/0.04) and (0.18/0.10), and MgAlSn (0.22/0.04) and (0.20/0.07). The curves are shifted for clarity.

3.2.2. Mössbauer Spectroscopy. ^{119}Sn solid-state NMR technique was performed on the samples, but because of the large chemical shift anisotropy, it leads to a low sensibility even though proton decoupling technique is used. Velu et al. have shown that the values match the data recorded for SnO_2 showing that Sn is disposed into *Oh* site.[6] Despite that, they interpret the broadening of the resonance peak as a lowering of the local symmetry around the Sn nuclei and the presence of possible magnetic interaction with neighboring Al nuclei in the brucite-like layer. The Mössbauer spectroscopy appears here to be a suitable technique.

^{119}Sn Mössbauer spectra of two selected samples of each system, MgAlSn and CoAlSn, recorded at 293 and 80 K are displayed in Figure 8. The spectra exhibit curves similar to one another and which may be explained on the basis of an environment for Sn atoms characteristic of SnO_2. The Mössbauer parameters are summarized in Table 3. The values of isomer shift in the range of −0.02 to 0.07 mm/s relative to $BaSnO_3$ are unambiguously characteristic of a tin^{IV} oxidation state in 6-fold coordination. Quadrupole splittings in the range of 0.48−0.49 mm/s outline a slight distortion of the local tin coordination, and comparison of these values with the hyperfine parameters of SnO_2 ($\delta = 0$ and $\Delta = 0.50$ mm/s) shows that the tin short local order is of the same type as that for SnO_2.[30] The greater amplitude in a Sn-containing MgAl sample compared to CoAl indicates the presence of more rigid framework

Table 3. Mössbauer Parameters of the Sn-Containing Samples at 293 and 80 K; $BaSnO_3$ Was Used as Reference for the Isomer Shift (δ)

compound	T (K)	δ (mm/s)	Δ (mm/s)	Γ (mm/s)	absorption (%)
Co_3AlSn_{15}	293	0.017 (4)	0.481 (7)	0.85 (1)	1.08
$(0.23/0.04)^a$	80	0.067 (3)	0.487 (6)	0.882 (9)	3.96
Co_3AlSn_{30}	293	0.029 (3)	0.489 (6)	0.871 (9)	2.53
$(0.18/0.10)^a$	80	0.066 (3)	0.481 (5)	0.901 (8)	5.79
Mg_3AlSn_{15}	293	−0.015 (2)	0.485 (3)	0.854 (5)	2.67
$(0.22/0.04)^a$	80	0.030 (3)	0.488 (6)	0.886 (9)	5.93
Mg_3AlSn_{30}	293	−0.014 (4)	0.473 (6)	0.873 (9)	4.58
$(0.20/0.07)^a$	80	0.020 (3)	0.477 (5)	0.879 (8)	10.00
"SnO_2"[b]	293	0.02 (7)		1.4 (2)	
	80	0.04 (3)	0.53	0.72 (8)	

[a] ($^x/_y$) taking into account both hypotheses, $M^{II} - M^{III}$ or $M^{III} - M^{IV}$ substitution according to $x = 1/(1 + \beta_{exp})$ with $\beta_{exp} = M^{II}/Al$, and $y = 0.25 \times \alpha_{exp}/(1 + \alpha_{exp})$ with $\alpha_{exp} = M^{IV}/Al$ (see text). [b] Material prepared in the absence of divalent and trivalent cation (see text).

in the first case. As expected, such a trend is also observed when the temperature is lowered to 80 K.

In the hypothesis of the Sn cations present in the sheets, one should expect magnetic interactions between Sn and the paramagnetic Co^{II} (3d7), different from those present in the MgAlSn matrix, and which would have been revealed by a broadening of the Mössbauer spectra. Again, one can conclude that the Sn cations are not directly incorporated in the LDH sheets. The Mössbauer spectrum was recorded on material prepared in the absence of divalent and trivalent cations, and the characteristics are close to those of SnO_2 (Table 3).

The textural properties of the Sn-containing samples are similar to those of samples prepared in the absence of tetravalent cations. A "sand-rose" morphology is observed by SEM, and the platelets are "glued" together by smaller particles when tetravalent cations are incorporated in the preparation.

When divalent and trivalent cations are absent from the preparation, a white powder is obtained for M = Sn and Zr. Amorphous at room temperature, the materials crystallize into SnO_2 (PDF file 41-1445) or ZrO_2 (PDF file (14-0534) at ~1000 °C.

4. Conclusions

From all the results, we can conclude that the incorporation of tetravalent cations does not occur; rather, an amorphous $M^{IV}O_2$-like oxide is formed, impregnating the LDH crystallite as observed in other systems,[31] and thus explaining the catalytic properties observed previously.[7]

The first metallic coordination sphere at the tetravalent K-edge is mainly dominated by $M^{IV}-M^{IV}$ correlation, dismissing their presence in the sheets of LDH.

Previous results have to be explained as follows: (i) The variation of the interlamellar distance is not due to an increase of the layer thickness under strong corrugation, but rather due to a change in the layer density. As observed experimentally, a decrease in the electrostatic attraction (lower Al content) forces between hydroxide layers and the interlayer anions increase the basal spacing. (ii) Formation of the LDH phase is thermodynamically more favorable than $MgSn(OH)_6$, this phase starts to emerge when the ratio Mg/Al is too large for the formation of LDH, the excedent Mg^{II} reacting then with the Sn^{IV} source. (iii) Precipitation of $SnCl_4$ and zirconyl nitrate precipitation, alone, gives rise to amorphous materials, whereas precipitation of $SnCl_4$ in aqueous ammonium at pH of 11 gives rise to ill-defined SnO_2-type glasslike monolithic xerogel. (iv) MgAlM (M = Zr and Sn) present a "memory effect", as the lamellar structure is fully reconstructed after thermal treatment at 400 °C, lower than the temperature of $M^{IV}O_2$ crystallization. The local order arond Zr or Sn is not modified. (v) The presence of M^{IV} oxide coating the LDH crystallite stabilizes their microstructural properties and allows also the formation of LDH with low Al content, although an amorphous component cannot be avoided for a ratio of M^{II}/Al greater than 4.

Finally, preliminary results for the system Co_2AlTi demonstrate a similar behavior, that is to say a segregation of the Ti^{IV} cations from the LDH phase to form TiO_2-type particles,[32] in disagreement with previous expectations.[33]

Acknowledgment. We thank Dr. Valérie Briois and Anne-Marie Flank for their help in recording the XAS data, and LURE for the use of the facilities.

CM0304039

(30) Stevens, J. G.; Goforth, M. A.; Boss, C. R.; Green, S. C.; Thurston, E. N., Eds.; *^{119}Sn Mössbauer Handbook: References and Data*; Mössbauer Effect Data Center: Asheville, NC, 1993.

(31) Harrison, P. G.; Bailey, C.; Bowering, N. *Chem. Mater.* **2003**, *15*, 979.

(32) Intissar, M.; Holler, S.; Malherbe, F.; Besse, J.-P.; Leroux, F. *J. Phys. Chem. Solids*, in press.

(33) Taylor, R. M. *Clay Miner.* **1984**, *19*, 591.